The Temperature Dependent Far-Infrared Analysis Of Purine Nucleic Acid Compounds

S Lappi [1], N Marinkovic[2], M Chance[2], and S Franzen[1]
[1]Dept. of Chemistry, North Carolina State University, Raleigh, NC.
[2]Dept. of Physiology And Biophysics, Albert Einstein College Of Medicine, Bronx, NY.

Hydrogen bonding is the crucial element that leads to molecular recognition in DNA and RNA. Deoxyribonucleic acid (DNA) and Ribonucleic acid (RNA) are biopolymers whose secondary structure depends in large measure on recognition of hydrogen bond patterns. The classic Watson and Crick model of DNA requires an internal set of hydrogen bonds, which align opposing nucleotides, and specific patterns of hydrogen bonding must be satisfied if two complementary (or nearly complementary) strands are to form an element of secondary structure. Base stacking stabilizes the B-form of helical DNA, one of the most widely recognized structures on the planet. While this fact and certain correlations based on calorimetry have great predictive value for the melting temperature of particular DNA sequences, the molecular details of the energetics of molecular recognition due to hydrogen bonding is still an area of active research. This research has great importance in understanding drug interactions, the effect lesions, and formation of higher order structures using DNA or RNA templates.

Despite the great interest in the structure and dynamics of polynucleotides, very little spectroscopic work has been done in the far-infrared region. The far-infrared is a region of the spectrum in which low frequency vibrational motions are found. Hydrogen bonding and large dynamical molecular motions are generally found in this region of the spectrum. Thus, far-infrared spectroscopy provides a method for the investigation of the hydrogen-bonding environment of a molecular system. Moreover, the temperature dependence of low frequency modes reveals their anharmonic coupling. As the temperature is lowered, the ground state population increases relative to all excited states. For an anharmonic transition, the energy gap between any two successive vibrational states gets smaller as the vibrational quantum state increases. Thus, as the population of the ground state increases the frequency of the vibrational transition increases. We use the temperature dependence as evidence for anharmonic coupling.

All too often, the infrared spectrum of a compound contains significantly more bands than can be accounted for by normal coordinate analysis. There are several reasons for this discrepancy: combination bands, mixing and splitting of solute and solvent bands and overtones that become allowed due to anharmonicity. Stable isotopic substitution of central and peripheral atoms provides a means to alter the vibrational pattern to facilitate comparison with calculation. Using a comparison of experiment and calculation, we can identify modes that are anharmonically coupled to low frequency hydrogen bonding modes. In this way, a check is obtained on the potential energy surfaces that we calculate for the hydrogen bonding interactions in nucleic acids.

Natural abundance adenine and 2-deoxyadenosine were purchased from Sigma Chemical Company, St. Louis, MO. Isotopic adenine was singly labeled with ^{13}C at positions C(2) & C(8), with ^{15}N at exocyclic amino (N(6)) & N(9), and triply labeled with ^{13}C at C(8) and ^{15}N at N(6) & N(9). Isotopic 2-deoxyadenosine was singly labeled with ^{15}N at exocyclic amino (N(6)) & N(9), doubly labeled with ^{13}C at C(8) and ^{15}N at N(9), and triply labeled with ^{13}C at C(8) and ^{15}N at N(6) & N(9). Both sets of isotopic compounds were obtained from the Stable Isotope Resource at Los Alamos National Laboratory. Deuterated derivatives of adenine and its isotopomers were prepared by way of hydrogen exchange reflux, for a minimum of 4 hours, at 40°C in D_2O (Aldrich Milwaukee WI. 99.9%). De-ionized 18MΩ water exchange was performed on all six samples of adenine as a control.

Polycrystalline samples were placed between two polyethylene windows of dimensions 7mm diameter X 0.8mm thick and then mounted in the sample holder of a liquid helium cold finger (Janis ST-100). The temperature was monitored by a Lake Shore Cryotronics

temperature controller (DRC-82) using a silicon diode sensor mounted above the sample holder. The cold finger was placed into its heat shield base, which had been mounted in a vacuum box that maintained a vacuum of approximately 100 mTorr. The vacuum box was connected to a dry nitrogen purged Nicolet Magna FTIR spectrometer (model 860), with a mirror velocity of 633 Hertz and a liquid helium cooled boron-doped silicon bolometer (Infrared Lab, Arizona). The synchrotron radiation beam of beamline U2B at the NSLS was the light source for these experiments. The effective spectral window provided by this experimental setup is 40 cm^{-1} to 600 cm^{-1}. The molecular structures for adenine and 2-deoxyadenosine are given in Figure 1.

A temperature-dependent series of far-infrared absorption spectra, from 80 to 300 K, of adenine are shown in Figure 2. The important features to note are the shifts and sharpness of the bands that occur as a result of changing temperature. Also of interest is the appearance of new bands in the 80K spectra that are poorly resolved in the 300K spectra. The appearance of these new bands is believed to be the result of anharmonic coupling of low frequency modes in this polycrystalline material.

A temperature-dependent series of far-infrared absorption spectra of 2-deoxyadenosine is shown in Figure 3. Whereas the number of peaks is greater than for adenine owing to the presence of ribose, the bands at 104 cm^{-1}, 139 cm^{-1}, 247 cm^{-1}, 336 cm^{-1} and 542 cm^{-1} are the same in both compounds. Good agreement with experimental vibrational frequencies at 10 K can be obtained using Density Functional Theory calculations. These calculations and extensive isotope labeling are being used to determine the strength of

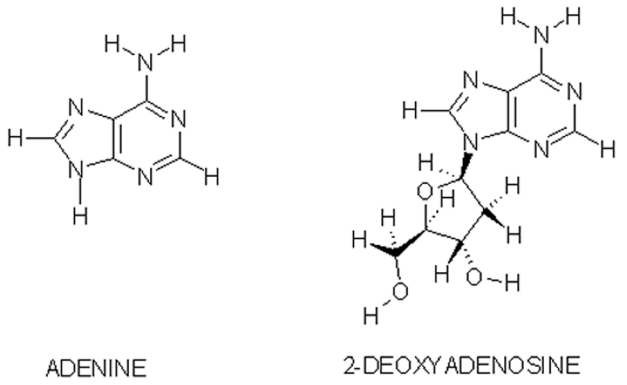

Figure 1: Molecular structure of the adenine and 2-deoxyadenosine.

anharmonic coupling for the modes shown in Figures 2 and 3.

The fact that so many low frequency modes appear to have strong temperature dependence is something of a surprise. Given the studies of anharmonic coupling in other biological molecules (e.g. the axial vibrations of the heme iron in heme proteins) one might have expected only one or two of the modes to show significant anharmonic coupling. The fact that so many modes show temperature dependence (i.e. anharmonic coupling) has slowed efforts to identify relationships that are unique to the hydrogen bonding interaction. The goal of future studies is to obtain similar data in oligonucleotides in crystalline and glassy forms in order to determine the effect of hydrogen bond patterns on vibrational spectra in the far-infrared region.

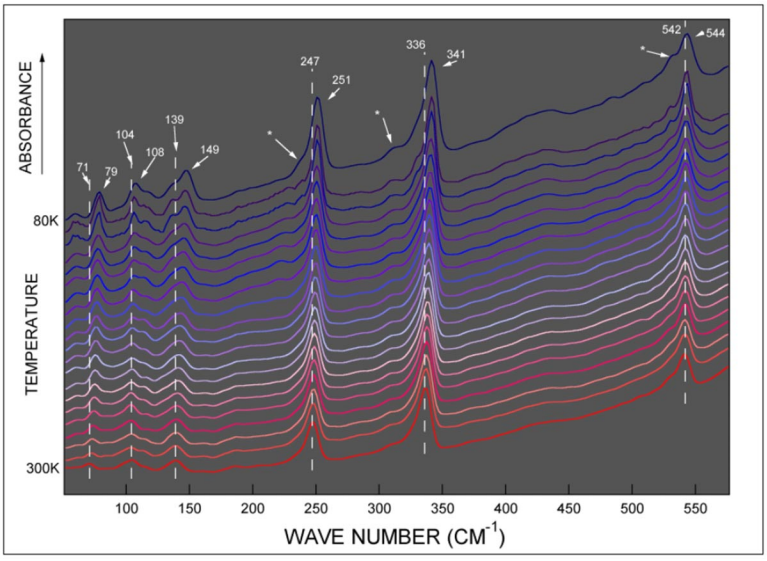

Figure 2: Temperature-dependent series of far-infrared absorption spectra of polycrystalline natural abundance adenine. The temperature range is in 10K increments from 80K to 300K. The spectra for 110K and 100K have been left out for clarity. The bands indicated by "" symbols are poorly resolved in the 300K spectra, but are clearly present in the 80K spectra. The data are not corrected for changes in source intensity.*

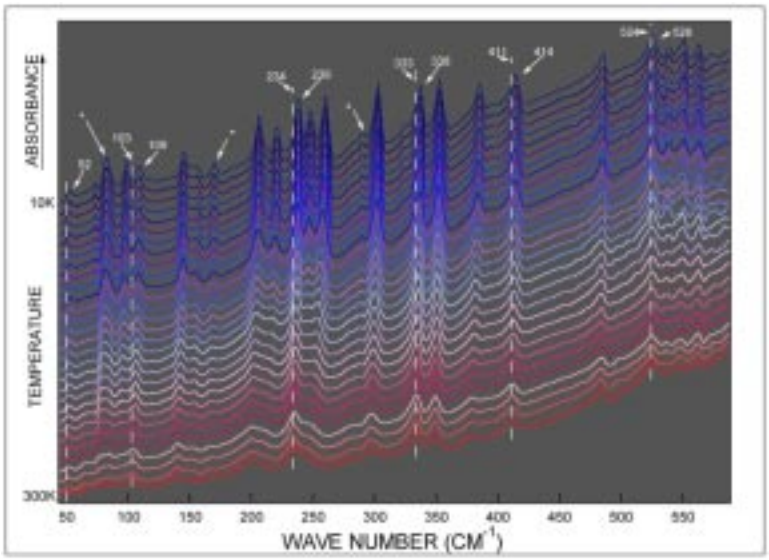

Figure 3: Temperature-dependent series of far-infrared absorption spectra of poly-crystalline natural abundance 2-deoxyadenosine. The temperature range is in 10K increments from 10 to 300K. The bands indicated by "" symbols are poorly resolved in the 300K spectra, but are clearly present in the 10K spectra. The data are not corrected for changes in source intensity.*

Desulfurization Reactions on Oxide Surfaces: Photoemission and XANES Studies

José A. Rodriguez, Jan Hrbek, Joseph Dvorak and Tomas Jirsak
Department of Chemistry, Brookhaven National Laboratory

In chemical feedstocks derived from petroleum or other natural sources, sulfur--containing molecules are common impurities [1]. These impurities are responsible for the poisoning of catalysts used in many chemical and petrochemical processes [2]. In addition, they constitute a major environmental problem due to the generation of sulfur oxides during the burning of fossil-derived fuels [3]. Metal oxides play an important role when dealing with the negative effects of sulfur [2]. On one hand, metal oxides are widely utilized as catalysts or catalyst supports in industrial operations and are poisoned by sulfur. There is a general desire to increase the sulfur tolerance of these oxide-based catalysts. On the other hand, many oxides are used as sorbents of S-containing molecules in oil refineries and in the destruction or removal of SO_2 (DeSOx process). Thus, for practical reasons, it is necessary to obtain a fundamental understanding of the behavior of sulfur on oxide surfaces [2].

TiO_2 is employed on a large industrial scale for the removal of H_2S in the Claus process [4]. Little is known about the elementary steps of the original Claus reaction ($H_2S + 1/2O_2 \rightarrow H_2O + 1/nS_n$) and its latter modification, where one third of the H_2S is first burned ($H_2S + 3/2O_2 \rightarrow SO_2 + H_2O$) and SO_2 reacts catalytically with the rest of the H_2S ($2H_2S + SO_2 \rightarrow 2H_2O + 3/nS_n$) [4]. Recently, we have carried out a detailed investigation of the adsorption of sulfur on a TiO_2(110) single crystal [5]. Figure 1 shows a model for this surface. On this system sulfur can interact with several adsorption sites: titanium, in-plane oxygen, bridging oxygen, and vacancies in the bridging oxygen rows. Figure 2 shows S 2p photoemission spectra acquired after dosing S_2 to a TiO_2(110) surface at 300 K. When similar experiments were done with a commercial source of X-rays, only a broad (~ 6 eV) peak was observed in the S 2p region [6]. In experiments at beamline U7A of the NSLS, we were able to identify four different types of sulfur species on the TiO_2(110) surface. For the smallest dose of S_2 in Figure 2, a doublet is observed with the S $2p_{3/2}$ features at ~ 161.8 eV. This peak position corresponds to S atoms bonded to O vacancies in the bridging oxygen rows of the TiO_2(110) surface [5]. Additional dosing of S_2 leads to a drastic change in the line shape of the S 2p spectrum. The resulting spectrum ("a") is well described by a fit with *four* doublets with $2p_{3/2}$ components at 161.6 (s_1), 162.8 (s_2), 163.3 (s_3) and 167 eV (s_4). For the fitting a Shirley background was subtracted from the raw spectrum, and a convolution of Lorentzian and Gaussian functions was used

for each peak [5]. In Figure 2, s_1 is assigned to S atoms on O vacancies. The difference in binding energy between s_2 and s_3 is only ~ 0.3 eV, and we assign these features to S atoms bonded to the Ti rows of the surface [6]. The s_4 is well matched to the S 2p binding energies observed for SO_x species [7], and could be attributed to SO_2 or more likely SO_3 [5,7] groups on the oxide. The amount of SO_x species present is very small and is probably generated near steps or defect sites on the surface. Most atoms in the bridging oxygen rows of the surface are not as reactive, so they produce insignificant amounts of SO_x species. Dosing with additional S_2 induces the growth of the s_3 peak, which becomes dominant. The S 2p spectrum obtained after saturation of the surface with sulfur at 300 K ("b" in Figure 2) was also well described by a set of four doublets (s_1, s_2, s_3, s_4 species). The s_2, s_3, and s_4 species were not strongly bound to the surface and desorbed at temperatures below 500 K. On the other hand, the S bonded to the oxygen vacancies (s_1) remained on the oxide up to temperatures as high as 800 K [5].

H_2S and S_2 mainly interact with the metal centers of TiO_2 [5]. In contrast, SO_2 preferentially reacts with the O centers forming SO_3 and SO_4 species [7,8]. Figure 3 shows a S K-edge spectrum acquired after adsorbing SO_2 on a TiO_2(110) surface at 300 K. No signal is seen for chemisorbed SO_2 on the Ti cations, and the typical peak for SO_4 appears near 2482 eV [7]. For the adsorption of SO_2 on MgO and ZnO, oxides also used frequently as sorbents/catalysts in desulfurization operations [2,4], one again finds SO_4 or SO_3 on the surface and no dissociation of the adsorbate [9,10]. On these oxides, the Mg-SO_2 and Zn-SO_2 interactions are too weak to lead to substantial bonding or dissociation of the molecule [9,10]. However, the Mg^{2+} and Zn^{2+} cations interact relatively well with H_2S

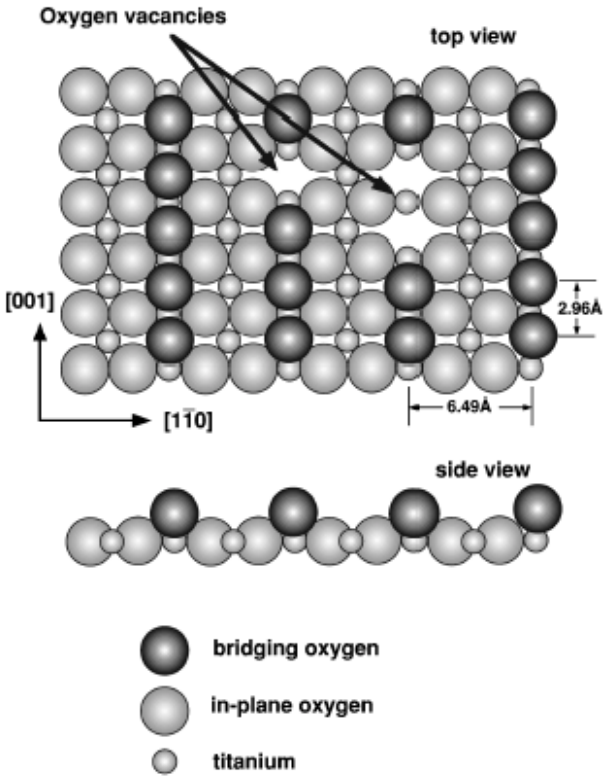

Figure 1. Model showing the different adsorption sites of a TiO_2(110) surface.

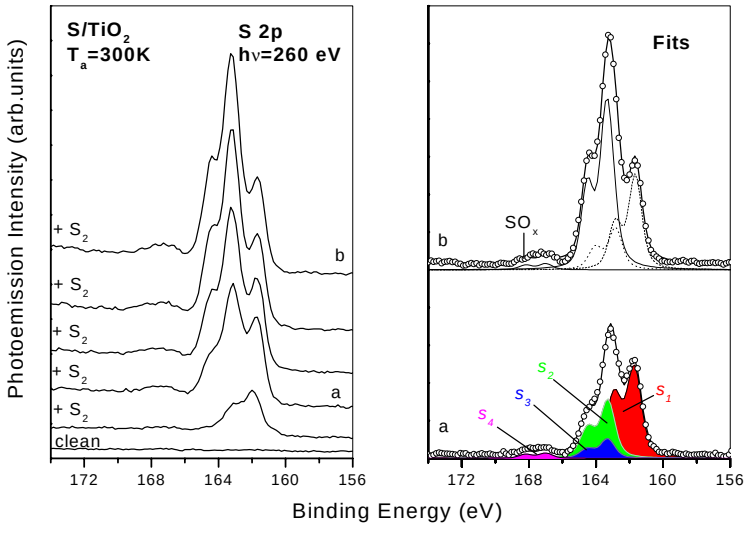

Figure 2. S 2p photoemission spectra for the adsorption of S_2 on TiO_2(110).

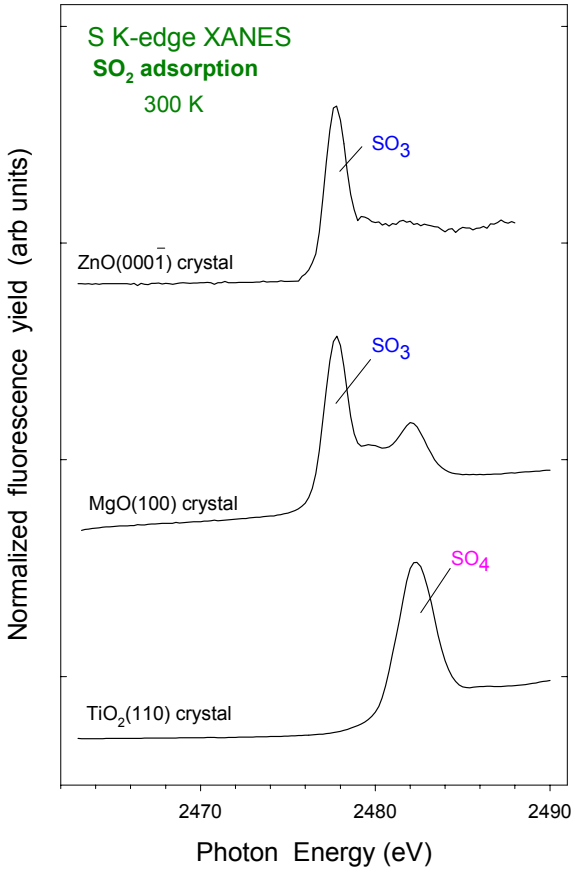

Figure 3. S K-edge XANES spectra for the adsorption of SO_2 on TiO_2(110), MgO(100) and ZnO(000$\bar{1}$)-O [8].

and S [11,12], as do the metal cations of TiO_2 (Figure 2).

The addition of an alkali metal to the surface of an oxide catalyst is a well-established procedure for enhancing the efficiency of oxides in DeSOx processes [2,3,10]. However, the exact role of the alkali in the removal process is not well understood. The alkali may be the real active phase or simply a promoter of the chemical activity of the oxide surface. Figure 4 shows S 2p photoemission spectra for the interaction of SO_2 with K/ZnO(000$\bar{1}$)-O and Cs/ZnO(000$\bar{1}$)-O. On pure ZnO(000$\bar{1}$)-O, only a doublet for SO_3 is detected. Upon coadsorption with K and Cs, the full dissociation of SO_2 takes place and a strong signal appears near 162 eV for S atoms. We have found that the surface chemistry of SO_2 on the alkali promoted oxides is complex, involving the coexistence of SO_4, SO_3 and S [10,13]. The alkali adatoms provide occupied electronic states above the oxide valence band that are very efficient for bonding and dissociating SO_2 [13].

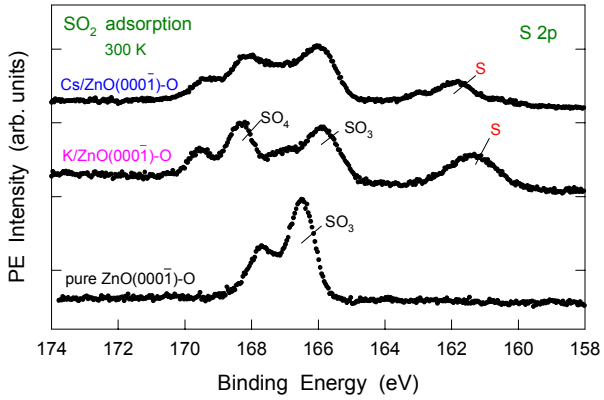

Figure 4. S 2p photoemission spectra for the adsorption of SO_2 on K/ZnO and Cs/ZnO at 300 K

Acknowledgements

This research was carried out at Brookhaven National Laboratory under contract DE-AC02-98CH10086 with the US Department of Energy (Division of Chemical Sciences).

References

1. J.G. Speight, "The Chemistry and Technology of Petroleum", 2nd Ed; Marcel-Dekker: New York, 1991.
2. J.A. Rodriguez and J. Hrbek, *Accounts of Chem. Research*, **32**, 719, 1999.
3. A.C. Stern, R.W. Boubel, D.B. Turner and D.L. Fox, "Fundamentals of Air Pollution", 2nd Ed.; Academic Press: Orlando, FL, 1984.
4. A. Pieplu, O. Saur, J.-C. Lavalley, O. Legendre and C. Nedez, *Catal. Rev.-Sci. Eng*. **40**, 409, 1998.
5. J.A. Rodriguez, J. Hrbek, J. Dvorak and T. Jirsak, *Chem. Phys. Lett*., submitted.
6. E.L.D. Hebenstreit, W. Hebenstreit and U. Diebold, *Surf. Sci*. **461**, 87, 2000.
7. D.R. Warburton, D. Pundie, C.A. Muryn, K. Prahakaran, P.L. Wincott, and G. Thorton, *Surf. Sci*. **269/270**, 305, 1992.
8. J.A. Rodriguez, M. Perez, T. Jirsak, L. Gonzalez, to be published.
9. J.A. Rodriguez, T. Jirsak, A. Freitag, J.Z. Larese and A. Maiti, J. Phys. Chem. B, **104**, 7439, 2000.
10. J.A. Rodriguez, T. Jirsak, S. Chaturvedi and M. Kuhn, *Surf. Sci.* **442**, 400, 1999.
11. J.A. Rodriguez and A. Maiti, *J. Phys. Chem. B*, **104**, 3630, 2000.
12. J.A. Rodriguez, T. Jirsak, M. Perez, S. Chaturvedi, M. Kuhn, L. Gonzalez, and A. Maiti, *J. Am. Chem. Soc*. **122**, 12362, 2000.
13. J.A. Rodriguez, T. Jirsak and J. Hrbek, *J. Phys. Chem. B*, **103**, 1966 (1999).